



“Gheorghe Asachi” Technical University of Iasi, Romania



SNOW EVAPORATION CHARACTERISTICS RELATED TO MELTING PERIOD IN A FORESTED CONTINUOUS PERMAFROST REGION

Youwei Lin, Tiji Cai *, Cunyong Ju

College of Forestry, Northeast Forestry University, Harbin 150040, China

Abstract

In cold, high-latitude regions, snow evaporation can significantly influence the snow water equivalent and thus change the regional water balance in early spring. In order to explore how the snowfall event and environmental factors affected the snow evaporation rate in the northern Daxing'an Mountains in China. From the snow melting period of March 2016 to April 2018, the eddy covariance method was used to explore the relationship between environmental factors and snow evaporation. The results showed that the air temperature played a more important role than net radiation in snow evaporation. The snow evaporation rates obviously increased after snowfall events during the snow ablation period, but the increments were different in different years. Throughout the observation period, the maximum snow evaporation was $0.448 \text{ mm} \cdot \text{d}^{-1}$ and occurred in the snow ablation period of 2016. However, the following processes induced an abrupt increase of snow evaporation rate: heavy snowfall events resulting from temporary warm air temperatures. Our results can be used to improve snowmelt models, and the corresponding routines in climate models, as well as can contribute to the development of more efficient practices of water resources utilization.

Key words: air temperature, eddy covariance, permafrost, snowfall, snow evaporation

Received: October, 2019; *Revised final:* February, 2020; *Accepted:* March, 2020; *Published in final edited form:* March, 2020

1. Introduction

As an essential element of the hydrologic cycle, evaporation plays an important role in the hydrological balance in mountain regions dominated by seasonal snow cover. The loss resulted from snow evaporation even accounted for 14-40% of the winter precipitation (Lundberg and Koivusalo, 2003). The fluctuations in snow-related variables (including snow evaporation, the infiltration of snow meltwater, and the snowmelt runoff) have profound effects on the hydrological processes in ecosystems (Alexander et al., 2010; Xu et al., 2017). For example, due to climate warming, air temperatures in montane regions were found to rapidly increase in early spring, and the rising air temperatures further accelerated snow evaporation as long as the snowpack remained (Herrero et al., 2016). Both the timing and volume of the annual snowmelt were also altered, and this alteration caused

water supply deficits in the dry spring season. Previous studies have focused on the influence of temperature and atmospheric energy changes on snow evaporation (Molotch et al., 2007; Pérez-Palazón et al., 2015), but the effects of specific snowfall events on evaporation have been neglected.

The thickness and duration of snowpack in the areas with frozen soil are greater than those in permafrost-free areas (Guo et al., 2018; Kokelj et al., 2017) since permafrost has unique radiation and thermodynamic characteristics that strongly affect the water/heat balance on the surface (Minderlein and Menzel, 2015). In contrast, the thaw of permafrost increases the soil water content and snow infiltration, decreases the spring snowmelt runoff and slows the regional warming trend (Helbig et al., 2016; Pal et al., 2018). However, permafrost areas are extremely sensitive to climate change (Smith et al., 2015). With global warming, the permafrost area in the

* Author to whom all correspondence should be addressed: e-mail: caitijiu1963@163.com; Phone: +0451-82191821

Daxing'anling Mountains - the second-largest permafrost region in China - has decreased by 35%, and the southern boundary of the permafrost region has receded 50 -150 km to the north (Jin et al., 2007). At the same time, the distribution of *Larix gmelinii*-the zonal climax vegetation - has undergone severe northward withdrawal over the last 50 years and is predicted to disappear from China by 2100 (Li et al., 2006). The degradation of permafrost and forest areas would lead to future changes in the ability of the snowpack to store water and impact the seasonal runoff patterns in snowmelt-dominated regions (Barnett et al., 2005). Therefore, the key hydrological processes occurring at the interface between the snowpack and the atmosphere have received increasing attention (Jones et al., 2014; Sexstone, 2016). There is agreement that snowpack and permafrost are vitally influenced by the water and energy budgets in the cold season at the land surface and in the atmosphere (Phillips and Schweizer, 2007).

In seasonally snow-covered coniferous forests, almost 60% of the total snowfall mass is intercepted by the forest canopy (Molotch et al., 2007) and 25-45% of the snowfall sublimates directly to the atmosphere (Pomeroy et al., 1998). Consequently, evaporation rates and the magnitude of spring snowmelt can be changed by the forest canopy due to the redistribution of radiant and turbulent fluxes (Molotch et al., 2007). Studies have shown that the mean maximum snow water equivalent in pine forests is 5-35% less than that in open areas (Gelfan et al., 2004). Compared with non-forested landscapes, forest cover alters the lower average snow accumulation and lower average melt rates (Faria et al., 2000; Storck et al., 2002; Winkler et al., 2005). Talbot et al. (2004) found that the melt rate in a non-forested area was 61% greater than that in a forested area. Other scholars also found that as the distance from stems decreased, the snow melting rate increased in a forest area (Pomeroy and Dion, 1996).

However, the interactions between forest and snow are still complex and poorly understood (Zhang et al., 2003). Although many studies have estimated snow evaporation from snowpack in large-scale forest areas (Guo et al., 2018; Fayad et al., 2017; MacDonald et al., 2018; Tor-ngern et al., 2018), few studies have focused on small-scale areas in high-latitude boreal forests. In China, studies related to snow hydrological processes have mainly been conducted on the Qinghai-Tibet Plateau, Tianshan Mountains (Liao et al., 2013) and Changbai Mountains (Li et al., 2013). The Daxing'anling Mountains are sensitive to climate change; however, this area has rarely attracted the attention of researchers.

This paper considered the particular status of the Daxing'anling Mountains and explored how a snowfall event affected the snow evaporation rate in this high-latitude, forested, permafrost region. Particularly, the objectives of this study were to (1) reveal the characteristics of snow evaporation before and after a snowfall event, (2) determine the influence

of a snowfall event on snow evaporation rates during the snow cover and snow melting periods, and (3) determine the main factors that affect the snow evaporation rates in winter to early spring, especially during the periods before and after a snowfall event. Given these aims, we use three winter datasets observed from the eddy covariance tower at the Mohe Forest Ecosystem Research Station in Northeast China. Our results could provide insights into the local winter hydrological characteristics as well as a database that can be used to establish a polished hydrological model.

2. Material and methods

2.1. Experimental sites

The study was conducted in the continuous permafrost region at the Heilongjiang Mohe Forest Ecosystem Research Station in the Daxing'an Mountains (122°20'06" E, 53°27'59" N) (Fig. 1a). The study site is characterized by a typical temperate continental climate with obvious mountainous climate characteristics, i.e., long cold winters and short warm summers. The average annual temperature is -3.8°C , and the mean monthly maximum temperature is 18.4°C in July, while the mean monthly minimum temperature is -30.9°C in January.

The annual precipitation is 431.2 mm, and it is mostly concentrated from June to September. The annual average frost-free period is 85-110 days. In the region, snowpack covers the surface of the land from October to April. The annual total solar radiation is $401.93\text{-}447.89\text{ kJ cm}^{-2}$, and the annual number of sunshine hours' ranges from 2377 to 2625 h in the region. The zonal vegetation of the region is bright coniferous forest, with *Larix gmelinii* being the dominant tree species. Other species include *Pinus sylvestris* var. *mongolica*, *Betula platyphylla*, and *Populus davidiana*. According to the data collected via a wooden ruler, the average DBH of the *Larix gmelinii* forest is 10.22 cm, and the average tree height is 12.11 m. The average DBH of other tree species is 10.21 cm, and the average tree height is 8.31 m. In this plot, the forest density is 1530 plants/hm². The soil is dominated by coniferous forest soils ranging from 20 to 30 cm in thickness, with a top organic layer that is between 0.05 and 0.2 m thick. The soil layer is between 1.0 and 3.0 m thick and is composed of a mixture of sandy clay, gravel and permafrost (Duan et al., 2014) (Table 1). In general, and in mountainous areas, snow is always considered a nonuniform surface. The presence of patchy snowpack in the forest and other obstacles such as forest cover, rocks, and shrubs that emerge from the snow surface could impact the snowpack depth differences. For example, the peak of the snow depth varies widely between the snow accumulation period and the snow ablation period because forest cover, air temperature, and snowfall events can change the temporal and spatial characteristics of snow depth.

Table 1. Soil information for the experimental sites

Research Area	0–10 (cm depth)	10–20 (cm depth)
Sand (%)	80.8	93.6
Silt (%)	0.47	0.26
Clay (%)	2.94	1.59
Organic (%)	2.7	1.9
Bulk Density (g/cm ³)	1.13	1.19

On the other hand, the forest canopy always intercepts snowfall during snowfall days, which results in differences in the snow water equivalent (SWE) transfer and snow depth variation of 57% and 72%, respectively, between snow accumulation and ablation periods (Varhola et al., 2010). However, in this area with *Larix gmelinii* forest cover, the intercepted snowfall is limited in winter periods (leaves fall in autumn). The redistribution of snowdrifts over larger distances seldom occurs. Additionally, the uncertainty in the variability considered in this study is random.

However, the goal of this study was to reveal how snowfall controls the snow evaporation rate at the forest scale. The ways in which snowfall and forest canopy interception cause snow peak variations need more study in this area, which can be determined by integrating the variability over large scales.

The experiment was conducted from October 27, 2015, to May 2, 2016 (hereafter abbreviated to 2016) and from November 10, 2016, to April 20, 2017 (hereafter abbreviated to 2017), and from October 11, 2017 to April 30, 2018. The snow accumulation period (SCP) was defined as the continuous observation of snow stability, no significant snow melting phenomenon and a surface ground (0 cm) temperature that decreased by less than -0.2°C (Chen et al., 2011). This period includes October 15, 2015, to March 22,

2016, October 20, 2016, to March 2, 2017, and October 11, 2017 to March 17, 2018. The snow ablation period (SBP) was a period with a significant melting phenomenon before the arrival of spring, which was defined as the forestland surface temperature steadily increasing from -0.2°C . This period includes March 21, 2016, to April 30, 2016, March 3, 2017, to April 30, 2017, and March 18, 2018, to April 30, 2018. According to meteorological standards, snowfall is divided into small snow ($0 \leq \text{SWE} < 2.5$ mm), medium snow ($2.5 \text{ mm} \leq \text{SWE} < 5$ mm), heavy snow ($5 \text{ mm} \leq \text{SWE} < 10$ mm) and blizzard ($\text{SWE} \geq 10$ mm) snowfall levels (Yi et al., 2014).

2.2. Instrumentation and meteorological station

The eddy covariance, microclimatic and solar radiation instruments were installed on a 35-m height flux tower at the experimental site (Fig. 1b), and the measurement factors and others are shown in Table 2. The Mohe Forest Ecosystem Research Station was located near the tower, and snowfall data were collected from this station.

2.3. Environmental factors data

Based on the flux tower gradient meteorological system, the main environmental factors selected in this study include: R_n and snowfall (P) above 23 m canopy, air temperature (T_a), and relative humidity (RH) at 28 m canopy, wind speed and direction recorded by 36 m IRGASON. In the process of analysis, the study defined an observation day with snowfall occurrence (snowfall > 0.2 mm) as the snowfall day, and the observation day without snowfall occurrence (snowfall = 0 mm) as the non-snowfall day.

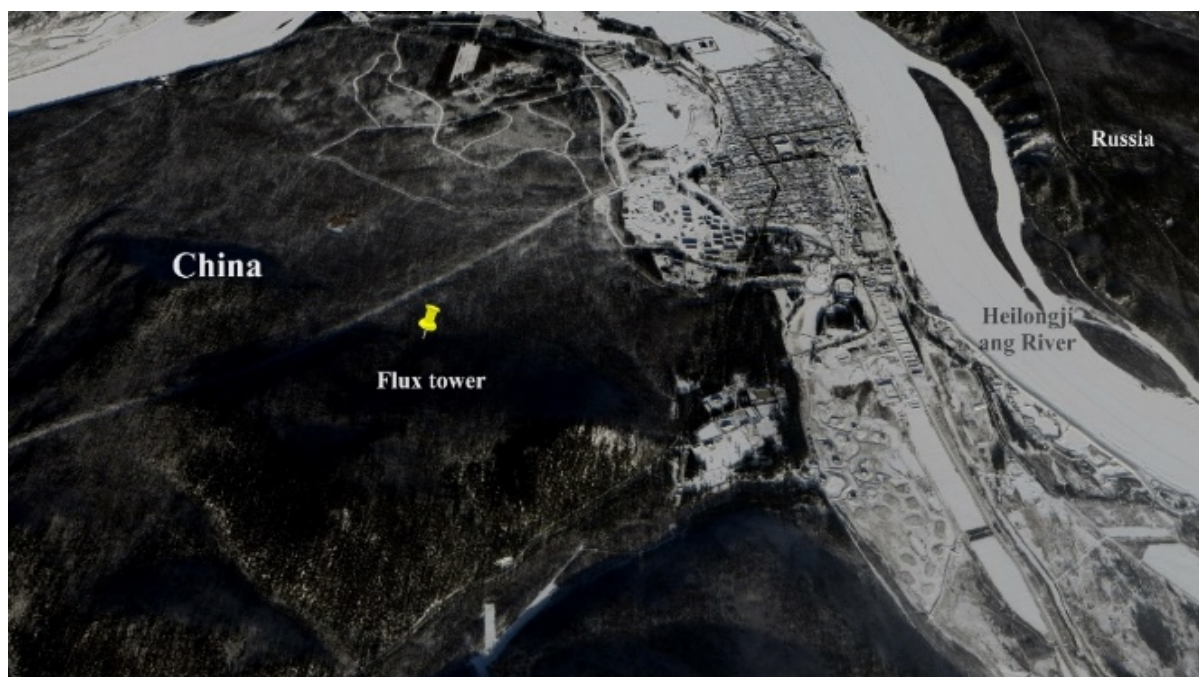
**Fig. 1.** A schematic plot of the research area including the coordinates of the forest sample and the flux tower

Table 2. The selected variables that were recorded by the eddy covariance, microclimatic and solar radiation instruments

Measurement Factor	Instrument	Height (+) or Depth (-)
Air temperature/humidity (T_a, e_a)	Campbell Scientific HMP45C capacitance hygrometer and thermistor	+28 m
Precipitation	TE525MM, Campbell Scientific, Inc., USA	+28 m
Wind speed (u)	Met One 014A 3-cup anemometer	+1.5, +9, +13, +20, +28, +35 m
Wind fluctuations (u', w')	Campbell Scientific CSAT3 ultrasonic anemometer	+28 m
Vapor fluctuations (q)	Campbell Scientific KH ₂ O hygrometer	+28 m
Net Radiation (R_n) (incoming/outgoing shortwave & longwave)	Kipp & Zonen CNR4 pyrometer and pyranometer	+28 m
Open-path EC system Latent heat flux Sensible heat flux (LE/H)	CSAT3, Campbell Scientific, USA Li-7500, LiCor Inc., USA	+28 m
Snow depth (P)	Campbell Scientific SSG snow depth gauge	0 m
Soil moisture (η)	Campbell Scientific CS616 water content reflectometer	-0.05, -0.1, -0.2, -0.4 m
Soil temperature (T_{s-0}, T_{s-5})	Type-T thermocouple wire	-0.05, -0.1, -0.2, -0.4 m
Soil heat flux (G)	Hukseflux HFT1 heat flux plate	-0.05, -0.1, -0.2, -0.4 m

2.4. Eddy covariance method

Energy balance closure is an important index to evaluate the quality of turbulent flux observation data in eddy correlation systems (Barr et al., 2006; Hiyama et al., 2007). During the snow ablation period, the energy that causes snowmelt originates from solar radiation and air temperature (Kelliher et al., 1997). In this paper, the energy balance ratio (EBR) is used to calculate the energy balance closure throughout winter as Eq. (1):

$$EBR = \frac{LE + H}{R_n - G - S} \quad (1)$$

where, LE is the energy flux of latent heat flux, H is the sensible heat flux, R_n is the net radiation, G is the change in heat storage in deep soil (5 cm below the surface) and S is the storage heat flux. Except for G , which was directly measured by the soil heat flux plate installed at a depth of 5 cm in the forest soil, the other parameters were calculated as follows. According to the methods of Constantin, Constantin et al. (1998) and Ohta et al. (2001), both the sensor path averaging error and the sensor separation error were ignored in this study.

The original 10Hz data during the observation was cut by date into data series at the interval of 30min with software LoggerNet (Campbell Scientific, USA); and the flux data calculated with software Eddypro (Li-Cor, USA). Main steps were as flows: outliers excluding, linear detrending, plane fitting, ultrasonic virtual temperature correcting, the effect of density perturbations, the test of turbulent stationarity, overall turbulent characteristics testing, data quality evaluation, data quality rating, etc. Meanwhile, software results were corrected as Xu et al. (2008) and Li et al. (2016) follows: the comprehensive sensitivity analysis of friction velocity (u^*) in this research (at the interval of 0.5m/s) found that, at any time during the observation, when $u^* < 0.20$ m/s, the turbulence was rather weak with an

impact on LE results, this part of data being therefore excluded. Degree of closure of the energy balance was the primary method for evaluation of the reliability of data observed with EC technology (Wilson et al., 2002).

(1) Latent and sensible heat flux

The eddy covariance method is a standard tool to obtain H and LE . According to the method described by (Brooks, 2008), a 3D rotation and a planar-fit rotation were first applied to force the average vertical wind speed (w) to zero and to align the horizontal wind (u) to mean wind direction (Mölder et al., 1999; Perez et al., 2008). Then, the average turbulent fluxes after each 30 min interval were calculated automatically by the built-in software (Campbell Scientific Inc.).

As the (Schmid et al., 2000) described, over 30 min periods, the vapor eddy covariance fluxes are calculated by the time series of the water vapor mixing ratio. The instruments have proposed the corrections of practical observations, such as the density, anemometer tilt, frequency response, and attack angle correction (Baldocchi et al., 2000; Finnigan et al., 2003; Horst and Oncley, 2006; Nakai et al., 2006). The covariances between vertical velocity fluctuations and either virtual temperature or water vapor are calculated by instrument (Campbell Scientific KH₂O hygrometer). Thus, LE and H were established as Eq. (2) and Eq. (3):

$$LE = \lambda \rho \overline{w'q'} \quad (2)$$

$$H = \rho C_p \overline{T'w'} \quad (3)$$

In both formulas, λ is the latent heat, $J\ kg^{-1}$, ρ is the water vapor flux, $kg\ m^{-2}\ s^{-1}$, q is the density of dry air, $kg\ m^{-3}$, w' is the vertical wind speed fluctuation, $m\ s^{-1}$, T' is the air temperature fluctuation, $^{\circ}C$, and C_p is the specific heat capacity of dry air (constant, $1013\ J\ kg^{-1}\ K^{-1}$). The λ , ρ , q' , w' and T' values were calculated from the measured soil temperature.

2.5. Storage heat flux

The storage heat flux S is indirectly estimated from four constituent components and can be defined as the Eq. (4) (Cho and Seok, 2008; McCaughey and Saxton, 1988):

$$S = S_a + S_w + S_s + S_g \quad (4)$$

In the formula, the S_g is the variation in the heat storage capacity of surface soil (5 cm above) (W m^{-2}) as Eq. (5) (Bartholdy, 2006):

$$S_g = C_s \cdot \frac{\Delta T_s}{\Delta t} \cdot h_s \quad (5)$$

where, Δt is the time interval, the value is 30 min; h_s is the thickness of the surface soil depth (5 cm), and ΔT_s is the average soil temperature (including 5 cm depth (T_{s-5}) and 10 cm depth (T_{s-10})), K. Those factors can be calculated directly from the flux tower measurements. C_s is the soil heat capacity ($\text{J m}^{-3} \text{K}^{-1}$), which was calculated as Eq. (6) (Oliphant et al., 2004):

$$S_g = \gamma_s \cdot C_m + \eta \cdot \gamma_w \cdot C_w \quad (6)$$

To obtain C_s , C_m is the specific heat of dry mineral soil (the value used here is $890 \text{ J kg}^{-1} \text{K}^{-1}$), γ_s is the dry soil bulk density (kg m^{-3}) (the value used here is 1100 kg m^{-3}), η is the volumetric water content in the soil (%), γ_w is the water density (the value used here is 1000 kg m^{-3}), and C_w is the specific heat of water in the soil (the value used here is $4190 \text{ J kg}^{-1} \text{K}^{-1}$). Second, S_a is the change in gas reservoir heat at the observed height, W m^{-2} . At the same time, S_a and S_w are the latent and sensible heat storage fluxes in the air column (W m^{-2}). S_a can be calculated as Eq. (7) and Eq. (8) (Oliphant et al., 2004):

$$S_a = \int_0^{Z_r} \rho' \cdot C_p \cdot \frac{\partial T_a}{\partial t} \cdot d_z \cong \rho' \cdot C_p \sum_{i=1}^n \left(\frac{\Delta T_a}{\Delta t} \cdot \Delta Z_i \right) \quad (7)$$

$$\rho' = \frac{P_a}{R_d(T_a + 273.5)(1 + 0.378e_a / P_a)} \quad (8)$$

Z_r represents the height of the eddy covariance sensor (28 m), R_d is the gas constant (the value is $287 \text{ J kg}^{-1} \text{K}^{-1}$), ΔZ_i is below Z_r . C_p is the specific heat capacity in dry air (constant, $1013 \text{ J kg}^{-1} \text{K}^{-1}$), T_a is the mean air temperature at a height of 1.5 m ($^{\circ}\text{C}$), P_a is the value of atmospheric pressure (kPa), and e_a is the water vapor pressure (kPa). T_a , P , and e_a are measured by the flux tower instruments. As in the method used to calculate S_a , the below-sensor air-space latent heat storage flux (S_w) is calculated as Eq. (9):

$$S_w = \int_0^{Z_r} \rho' \cdot \lambda \cdot \frac{\partial e_i}{\partial t} \cdot d_z \cong \rho' \cdot \lambda \cdot \sum_{i=1}^n \left(\frac{\Delta e_a}{\Delta t} \cdot \Delta Z_i \right) \quad (9)$$

where, e_i is the absolute humidity at 28 m (kg m^{-3}), which is measured by the flux tower instruments. Fourth, S_s is the heat storage flux (W m^{-2}) and the change in heat storage during snow cover. The latent heat flux S_s is calculated as Eq. (10):

$$S_s = \rho_{snow} \cdot C_{snow} \cdot \frac{\Delta T_{snow}}{\Delta t} \cdot h_{snow} \quad (10)$$

As for the SSG measurement data, ρ_{snow} is the average density of snow ($0.05 \cdot 10^3 \text{ kg m}^{-3}$), C_{snow} is the snow heat capacity ($2050 \text{ J} \cdot \text{kg}^{-1} \cdot \text{K}^{-1}$), T_{snow} is the snow temperature ($^{\circ}\text{C}$), and h_{snow} is the depth of the snow (m). Other parameters related to snowfall event were calculated by the snowfall data from the TE525MM, Campbell Scientific, Inc., USA.

2.6. Snow evaporation and regression analyses

In this study, the snow evaporation data before and after snowfall events are the data from three days before and after snowing. Linear regression analyses were used to explore the relationships between measured snow evaporation rates and cumulative net radiation, air temperature at this location for two years, and to quantitatively analyze the influence of cumulative net radiation and air temperature on the evaporation rate during the three years (snow ablation periods) before and after snowfall events.

Excluded the data 1h before and after every snowfall event, the intercepts, slope, statistical significance (p -value), and coefficient of determination (R^2) were evaluated during the winter period in this continuous permafrost region. The energy balance of forest ecosystems was generally $R_n = H + LE + G + S$. Due to the difference in determination instrument and spatial extent of radiation equilibrium and energy component, the two could hardly realize complete closure. In the research, through linear regression on the basis of $H + LE$ and $R_n - G$ per hour after quality control in the observation, it was obtained that the slope, intercept and R^2 of the equation were 1.56, 14.06 and 0.72 respectively.

3. Results

3.1. Meteorological conditions

The characteristics of snowfall, snow depth, snowfall intensity, snowfall class, and snowfall duration are shown in Fig. 2. The deepest depth in the snow period was 73.9 cm in 2016, 14.62 cm in 2017 and 22.27 cm in 2018. The snowfall events shown in Fig. 2a are largest and more frequent than those shown in Fig. 2b and 2c. During the snow ablation period, there were two blizzards in 2016, but only one light snow in 2017.

Only moderate snow and light snow events occurred in 2017. After the first snowfall event occurred during the snow accumulation period, the

snow depth increased rapidly but then decreased soon after (Fig. 2). When the third snowfall occurred, the snow depth began to increase steadily in both snow accumulation periods.

The total snowpack melting time in 2016 was longer than that in 2017. During the snow ablation period in 2016, after the snowfall events occurred, the average rate of the decrease in the SWE was 0.091 m d⁻¹, which was larger than that without snowfall events (0.023 m d⁻¹). This phenomenon was observed during the snow melting period of 2017 when only the magnitude of the rate of decrease was different from that in 2016, and it was 0.067 m d⁻¹ when snowfall events occurred and 0.033 m d⁻¹ when snowfall events did not occur. In 2018, the SWE decreased larger when the snowfall event happened during the snow ablation period. In addition, the snow ablation period appeared earliest in 2017 than in 2016 and 2018.

3.2. Diurnal variation in energy balance

The diurnal variation in the energy flux is shown in Fig. 3. After sunrise, the energy flux did not increase until 8:00. The value of every index peaked at midday and declined in the afternoon. The magnitude of the fluctuation in R_n was the greatest among the four indices. In addition, the values of these

four indices during the ablation period in 2016 was largest. But during both the years, these four indices followed a consistent order in terms of amount, and by rights the LE was larger than the H . As shown in Fig. 3a, the crest values of R_n , $G+S$, and LE occurred at 13:00, but the crest of H occurred one hour later. In the snow ablation period, the crest values of R_n and $G+S$ appeared from 12:00 to 13:00, while the crests of the LE and H lines appeared at 11:00. That is to say, except for the H with almost two hours delay in the ablation period.

3.3. Environmental conditions variation in different years

During the snow ablation period, an analysis of variance was performed with the evaporation rate of snow as the fixed variable and wind speed, net radiation, temperature and humidity as covariates; the results are as shown in Table 3. In Table 3, net radiation (R_n) and air temperature have significant effect on snow evaporation rate ($P < 0.001$); humidity and wind speed, on the other hand, are of less significant effect thereon. Later, the evaporation rate of snow was chosen to be a dependent variable in the response analysis on net radiation R_n and air temperature.

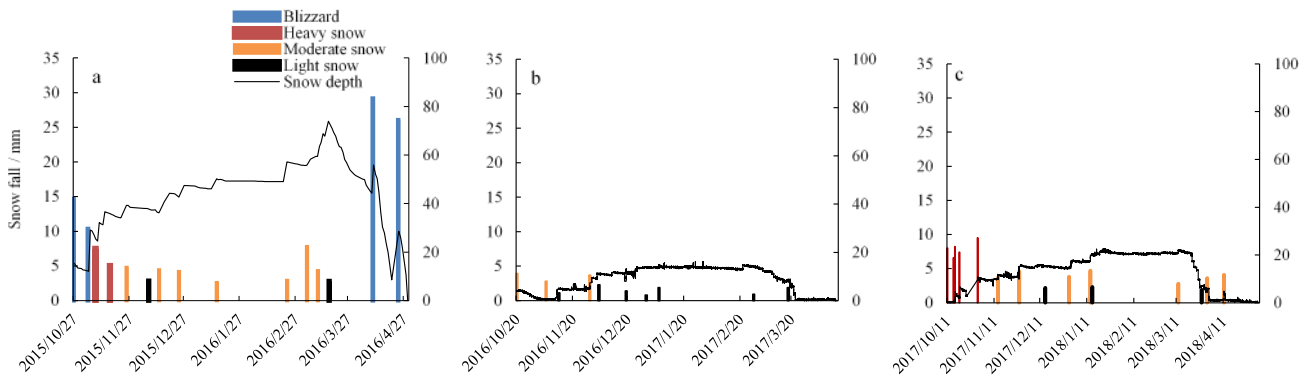


Fig. 2. Characteristics of snowfall and snow depth from: 2016-a, 2017-b and 2018-c

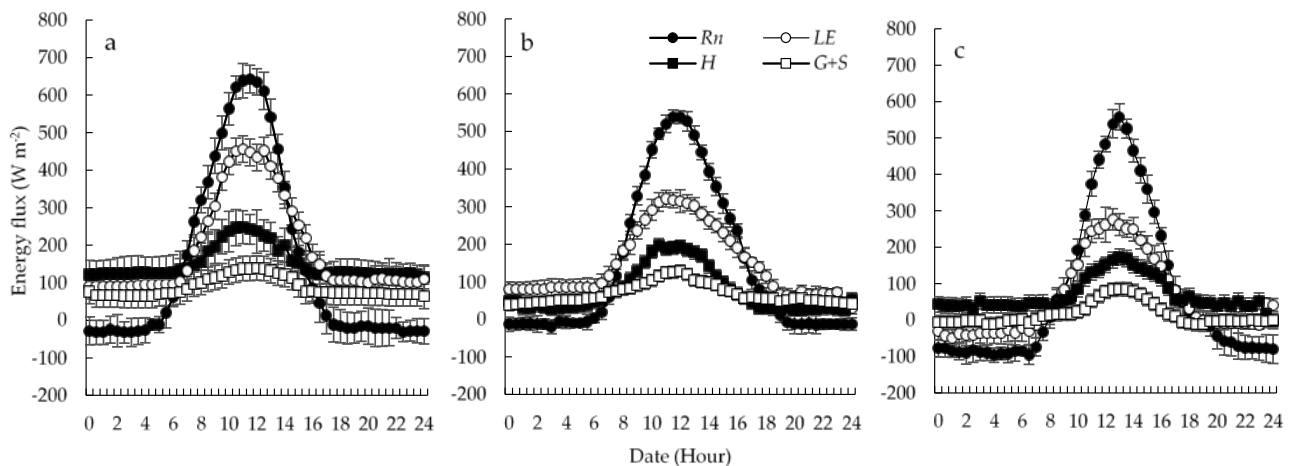


Fig. 3. Average diurnal net radiation flux (R_n), latent heat flux (LE), sensible heat flux (H), and storage heat flux ($G + S$) during the snow ablation period in 2016-a, 2017-b and c-2018

Table 3. The correlational relationship between snow evaporation rate and environmental factors

<i>i</i>	2016	2017	2018
	Snow evaporation rate	Snow evaporation rate	Snow evaporation rate
R_n (Net radiation)	$P<0.001$	$P<0.001$	$P<0.001$
Humidity	$P<0.005$	$P<0.005$	$P<0.005$
Wind speed	$P=0.043$	$P=0.118$	$P=0.025$
Air temperature	$P<0.001$	$P<0.001$	$P<0.001$

$n=2069$

The snow evaporation rates of two stages (after the snowfall and before the snowfall) were high in response degree to T_a (R^2 is 0.68 and 0.77; Fig. 4), and the T_a before the snowfall and after the snowfall was a limiting factor of the snow evaporation rate. In the time period after the snowfall occurs, the range of the gradual increase of the snow evaporation rate along with the increase of the T_a is more obvious compared with the time period before the snowfall occurs, and the snow evaporation rate in the snow ablation period could be accelerated when the air temperature was high. The snow evaporation rates and R_n in the two stages (after the snowfall and before the snowfall) are in positive correlation (Fig. 4), and R^2 in the stage before the snowfall was higher. After the snowfall occurs, the slope of a regression equation of the snow evaporation rate is lower than that in the stage before the snowfall occurs, which shows that the sensitivity of the snow evaporation rate along with the change of R_n was slightly higher before the snowfall event occurs (Fig. 4). The above results indicate that a snowfall increased the snow evaporation rate while also affecting the correspondence of T_a and R_n to the snow evaporation rate. In the snow ablation period, the influence of T_a on the water balance of an ecological system was more obvious.

3.4. Characteristics of the snow evaporation rate before and after snowfall events

The snow evaporation rate increased constantly during the snow ablation period. Although the total evaporation value in 2016 was largest in both three years, the characteristics of the evaporation fluctuation were similar (Fig. 5a, b and c). The net radiation

increased and remained steady in the beginning of the snow ablation period but later increased rapidly. Throughout the observation period, the highest evaporation value in both snow ablation periods was 0.448 mm d⁻¹ in 2016, the moderate value was 0.421 mm d⁻¹ in 2017, the smallest value was 0.29 mm d⁻¹ in 2018 (Fig. 5).

The snowfall events explicitly resulted in the increasing snow evaporation in both experimental periods (Fig. 5). In other words, the evaporation was lower before snowfall events than that after snowfall events. The differences between the years were significant at the $p < 0.05$ level. The mean snow evaporation rate during the snow ablation period before a snowfall event were 0.122 mm d⁻¹ in 2016, 0.144 mm d⁻¹ in 2017, and 0.51 mm d⁻¹ in 2018. whereas the mean evaporation rate after a snowfall event were 0.233, 0.229, and 0.186 mm d⁻¹ in 2016, 2017 and 2018, respectively. Furthermore, before a snowfall event, the snow evaporation rate of 2017 exhibited a smallest range in 2015-2018. After a snowfall event, the range of evaporation in the different years changed considerably.

4. Discussions

4.1. Energy fluxes and other environmental factors in snow ablation periods

The energy closure status of the EC system directly affects the evaluation of the evaporation, and compared to the FLUXNET (R^2 range is 0.64-0.95), the energy closure level (R^2 is 0.72) of the study site was within a reliable range, and could ensure a more ideal data quality.

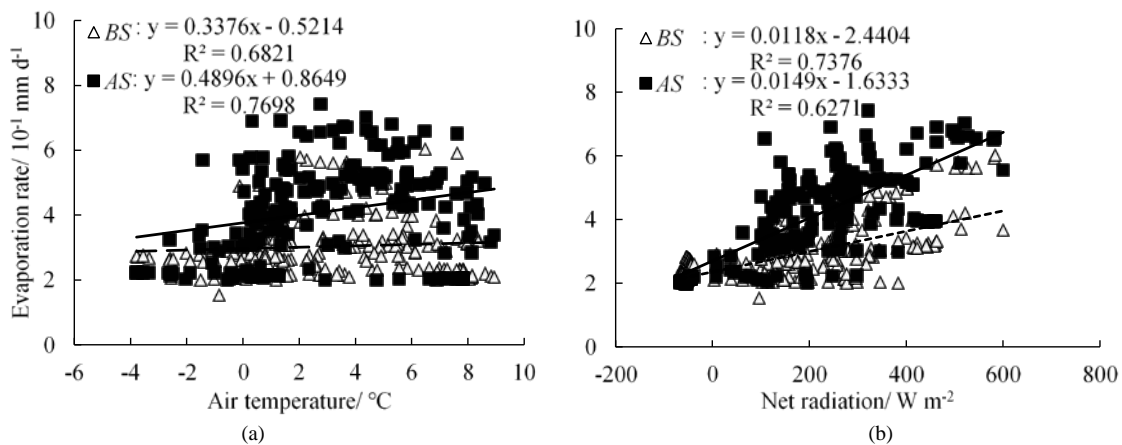


Fig. 4. Responses of snow evaporation to the (a) air temperature (T_a) and (b) net radiation (R_n) under different snowfall conditions. BS: Before snowfall days period; AS: After snowfall days period; All the equations in the figure are significant ($P<0.05$); $n=133$

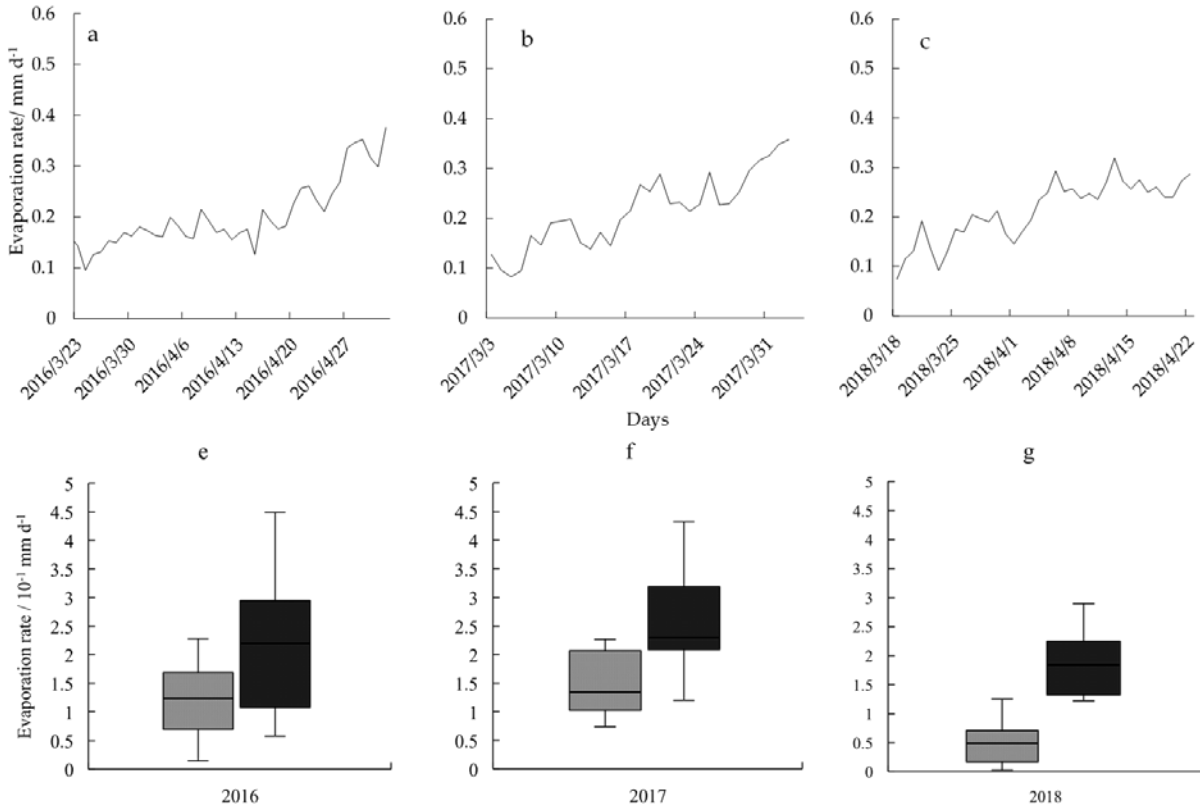


Fig. 5. The snow evaporation rate in 2016 (a), 2017(b), and 2018(c). The snow evaporation rate before (three days) and after (three days) snowfall events in the three snow ablation periods for 2016 (e). 2017(f) and 2018 (g). The white box indicates the values before snowfall event, the dark box indicate the values after snowfall event. n=133

Meanwhile, the *EC* technology easily underestimates the flux when the turbulence at night was insufficient, and the research eliminates data when the turbulence intensity was weak through a sensitivity test of u^* , which ensures that the measurement of an *EC* system was a result under the condition of strong turbulence while ensuring the integrity and continuity of the data (Goulden et al., 1996).

The difference in energy flux in the three snow ablation periods could indicate changes in both the air temperature and net radiation influenced the snow evaporation. Another report also supported the results of our experiment (Tanaka et al., 2008; Turnipseed et al., 2002). When the air temperature rises, the additional heat is used to melt the snowpack during the melting period. Fig. 4 and 5 shows that the evaporation rates during the snow ablation periods were dominated by air temperature and net radiation. In the early spring, the lowest temperature and associated coverage of snow-regulated water and heat variations caused the snow evaporation rates to remain almost unchanged (Nelson et al., 2014).

At the same time, compared with the effects of air temperature and net radiation, Jackson and Prowse (Jackson and Prowse, 2009) found that the snow evaporation rates in mountain regions were driven almost entirely by sensible heat fluxes during large-scale advection events. Previous studies have identified that atmospheric conditions are major

factors that affect the snow energy balance and evaporation. Other studies found that different snowfall levels and depths caused the heat flux to increase significantly during early spring, and this increase may occur simultaneously with the increase in the latent and sensible heat fluxes (Fratini et al., 2014). In this experiment, the air temperature in forests was higher during the day than at night, and transpiration and sensible heat flux exhibited large influences on forests (Fig. 3).

The snow evaporation rates in the different years were determined by net radiation and air temperature factors (Table 3). The factors were compared in the three years, which indicated that the significantly large snow evaporation rate in this area is probably attributed to the differences in the SWE and air temperature.

As shown in Table 3 and Fig. 4, in the snow ablation period, the crests of the R_n and $G+S$ lines appeared between 12:00 and 13:00. The crests of the LE and H lines appeared at 11:00. The minimum R_n value occurred between December and February at the latest and in April at the earliest, and the closure of the energy balance that was identified in this study appeared to be lower than that reported by others. This discrepancy related to the influence of the conditions of forests in a mountain region on the experimental results.

As shown in Fig. 4, the air temperature more significantly influenced the evaporation rates than the

net radiation in both snow ablation periods. These results were inconsistent with those observed in the Changbai Mountains (Li et al., 2013) and North America (Biederman et al., 2014). This difference related to the location of our study region. The main reason for this difference could be that the low temperature and freeze-thaw cycle in the frozen soil caused the forest to block the water vapor and heat that originated around the region, and the change in the turbulent flux of the vertical energy transfer to the atmosphere was very low (Lewkowicz, 2008). For these reasons, frozen soil may make the $LE + H + G + S - R_n$ values larger than those obtained by the values in the west of Daxing'an Mountains (the max values ranged from 77-79) (Chen et al., 2011).

4.2. Snowfall events and evaporation

In the snowpack period, the slightly warmer conditions in March and April 2016, in combination with the frequent occurrence of heavy snowfall events, resulted in high snow evaporation rates in this period. This result verified the results of the experiment by (Wang et al., 2013): the magnitude of the changes in snowfall may markedly affect the response of the snowpack to changes in snow evaporation. The snow evaporation rate in the spring of 2016 significantly increased during the snowfall event on April 10 (Fig. 5) and the subsequent snowmelt period (Fig. 5 and 6). The net radiation in the *Larix gmelinii* forests in this area indicated that the change in air temperature impacted snow evaporation during the winters of 2016, 2017 and 2018 (Fig. 5). The snowfall events could influence the snow evaporation in snow ablation period in different years. The variations in the snow evaporation rates were similar in both years. However, the snow evaporation rate in the melting period of 2017 and 2018 were less than that in the melting period of 2016 (Fig. 5). The main reason for this difference may be that less snowfall occurred in the spring of 2017 earlier than in the spring of 2016 and 2018, which caused the snowpack to disappear very early.

In this region, snow evaporation could result increase in the short term in the snow ablation period. Snow evaporation was larger after snowfall events than when snowfall events did not occur. Thus, the differences in snowfall events and air temperature in the snow ablation period were probably the main factors that resulted in the increase in the snow evaporation rate in this study area. Otherwise, the main factors that influenced the evaporation rate included R_n and air temperature (Lundberg and Halldin, 1994). After a snowfall event, the melting of snow requires the absorption of a large amount of energy, which promotes the effect of temperature on the snow during the evaporation period (Cohen, 1994). As shown in Fig. 5, after a snowfall event, the correlation between net radiation, temperature and the snow evaporation rate increased during the snowmelt period. Although other reports found that the physical properties of the snowpack during the snow melting

period could result in a 75% increase in net radiation thereby promoting the rate of decrease in the snowpack (Cline, 1997). However, in our experiment, a more significant correlation was found between the air temperature and snow evaporation. The main reason for this difference was that forest cover can decrease the surface energy flux and keep the air temperature warmer than that in areas without forest cover (Broxton et al., 2015; Nakai et al., 1999; Roth and Nolin, 2017). During the snow ablation period, the highest snow evaporation in 2016 was 0.448 mm, which was highest in 2017 (0.29 mm) and 2018 (0.421 mm). Thus, considering the prevalence of snowfall events (Fig. 2) and high snow evaporation (Fig. 2 and Fig. 6), these differences may account for the differences of snow evaporation in different years. It is likely that the physical properties of the new snowpack caused the energy flux to change and slightly increased the air temperature in this region. Another scholar also found that as the snow evaporation characters was influenced by the snowfall's aerodynamic resistance in the forest region (Lundberg et al., 1998). But the snow evaporation characterises always inconclusive because the environmental factors were unordered in different years (Male and Granger, 1981). The snow fall will change the energy which promoted the evaporation in the forested area (Saitoh et al., 2011). However, the law of snowfall changing snow evaporation rate in different regions has not been intensive studied. Long-term studies are needed to explore the relationship in snowfall, energy balance, and snow evaporation.

During the early spring, the heavy and new snowpack changed the ground-air energy flux (Jennings et al., 2018). Therefore, the following process should be the main reason why the snow rate changed during the snow cover and snowmelt periods in this area: (1) heavy snowfall events resulted from temporary and warm air temperatures and (2) the air temperature continuously increased by large amounts. Although our results are based on the data from a site, they clearly indicate the possibility that the snow evaporation changes. Because our results do not explain the entire process of evaporation with topography, further research is required to examine these details. Moreover, a special variant of the snow evaporation processes may largely influence the amount of snowmelt runoff that occurs in the spring (Tetzlaff et al., 2015). Although this study indicates the possibility that a large number of snowfall events influence the snow evaporation rate in the snow ablation period at the field scale, this experiment showed forest-scale field observations. More experiments are required over large-scale field areas to quantify the snow evaporation values during and after snowfall and snowmelt periods to ensure the rational utilization of forest water resources.

5. Conclusions

The long and low air temperature were the characteristics of the north of the Daxing'an

Mountains during the snow ablation period. When the snow ablation period began, the snow evaporation increased steadily. However, the temporary warm weather induced snowfall and caused a large release of snow evaporation into the atmosphere in a short time.

To quantify the relationship in environmental factors, snowfall, and snow evaporation, the distribution of snowmelt period of forests area in the permafrost region was determined. This study provided the scientific basic data for the characteristics of snow evaporation rate and the snowfall cause the evaporation rate changed in the north of Daxing'an Mountains during the snow ablation period. But our research didn't consider the possibility of soil heat flux input, melting water infiltration influence, and melting water runoff will change the snow evaporation rate during the snow ablation period.

The additional research was needed, including research on the differences in topography, an analysis of the evaporation model and a large-scale study. In order to provide the original data support for spring snowmelt water distribution mechanism and rational afforestation planning in this region.

Acknowledgements

This research was supported by the Forestry college of Northeast Forestry University and Heilongjiang Mohe Forest Ecosystem Research Station in the Daxing'an Mountains of Northeast China. This research was supported by the National Key R&D Program of China (2018YFC0507302), the National Science Foundation of China (Grant No. 31370460), the CFERN & BEIJING TECHNO SOLUTIONS Award Funds for excellent academic achievements of the Fundamental Research Funds for the Central Universities (2572018CP03), and Doctoral independent innovation fund project (2572016AA33).

f

References

- Alexander M.A., Tomas R., Deser C., Lawrence D. M., (2010), The atmospheric response to projected terrestrial snow changes in the late twenty-first century, *Journal of Climate*, **23**, 6430-6437.
- Baldocchi D.D., Meyers T.P., Wilson K.B., (2000), Correction of eddy-covariance measurements incorporating both advective effects and density fluxes, *Boundary-Layer Meteorology*, **97**, 487-511.
- Barnett T.P., Adam J.C., Lettenmaier D.P., (2005), Potential impacts of a warming climate on water availability in snow-dominated regions, *Nature*, **438**, 303.
- Barr A., Morgenstern K., Black T., McCaughey J., Nesic Z., (2006), Surface energy balance closure by the eddy-covariance method above three boreal forest stands and implications for the measurement of the CO₂ flux, *Agricultural and Forest Meteorology*, **140**, 322-337.
- Bartholdy J., (2006), A simple model for estimating current velocity in tidal inlets: example from Grådyb in the Danish Wadden Sea, *Geo-Marine Letters*, **26**, 133-140.
- Biederman J., Harpold A., Gochis D., Ewers B., Reed D., Papuga S., Brooks P., (2014), Increased evaporation following widespread tree mortality limits streamflow response, *Water Resources Research*, **50**, 5395-5409.
- Brooks I.M., (2008), Spatially distributed measurements of platform motion for the correction of ship-based turbulent fluxes, *Journal of Atmospheric and Oceanic Technology*, **25**, 2007-2017.
- Broxton P., Harpold A., Biederman J., Troch P. A., Molotch N., Brooks P., (2015), Quantifying the effects of vegetation structure on snow accumulation and ablation in mixed-conifer forests, *Ecohydrology*, **8**, 1073-1094.
- Chen N., Guan D., Jin C., Wang A., Wu J., Yuan F., (2011), Influences of snow event on energy balance over temperate meadow in dormant season based on eddy covariance measurements, *Journal of Hydrology*, **399**, 100-107.
- Cho K.R., Seok J.K., (2008), Correction on current measurement errors for accurate flux estimation of AC drives at low stator frequency, *IEEE Transactions on Industry Applications*, **44**, 594-603.
- Cline D.W., (1997), Snow surface energy exchanges and snowmelt at a continental, midlatitude Alpine site, *Water Resources Research*, **33**, 689-701.
- Cohen J., (1994), Snow cover and climate, *Weather*, **49**, 150-156.
- Constantin J., Inclan M., Raschendorfer M., (1998), The energy budget of a spruce forest: field measurements and comparison with the forest-land-atmosphere model (FLAME), *Journal of Hydrology*, **212**, 22-35.
- Duan L., Man X., Liu Y., Liu H., Tian Y., Liu X., (2014), Soil moisture spatial variability and affecting factors of natural larch forest in northern region of Daxinganling Mountains of northeastern China, *Journal of Beijing Forestry University*, **36**, 36-41.
- Faria D., Pomeroy J., Essery R., (2000), Effect of covariance between ablation and snow water equivalent on depletion of snow-covered area in a forest, *Hydrological Processes*, **14**, 2683-2695.
- Fayad A., Gascoïn S., Faour G., López-Moreno J.I., Drapeau L., Le Page M., Escadafal R., (2017), Snow hydrology in Mediterranean mountain regions: A review, *Journal of Hydrology*, **551**, 374-396.
- Finnigan J.J., Clement R., Malhi Y., Leuning R., Cleugh H., (2003), A re-evaluation of long-term flux measurement techniques part I: averaging and coordinate rotation, *Boundary-Layer Meteorology*, **107**, 1-48.
- Fratini G., McDermitt D., Papale D., (2014), Eddy-covariance flux errors due to biases in gas concentration measurements: origins, quantification and correction, *Biogeosciences*, **11**, 1037-1051.
- Gelfan A., Pomeroy J., Kuchment L., (2004), Modeling forest cover influences on snow accumulation, sublimation, and melt, *Journal of Hydrometeorology*, **5**, 785-803.
- Goulden M.L., Munger J.W., Fan S.M., Daube B.C., Wofsy S.C., (1996), Measurements of carbon sequestration by long-term eddy covariance: Methods and a critical evaluation of accuracy, *Global Change Biology*, **2**, 169-182.
- Guo W., Liu H., Anenkhonov O.A., Shangguan H., Sandanov D.V., Korolyuk A.Y., Hu G., Wu X., (2018), Vegetation can strongly regulate permafrost degradation at its southern edge through changing surface freeze-thaw processes, *Agricultural and Forest Meteorology*, **252**, 10-17.
- Helbig M., Wischniewski K., Kljun N., Chasmer L.E., Quinton W.L., Detto M., Sonntag O., (2016), Regional atmospheric cooling and wetting effect of permafrost thaw-induced boreal forest loss, *Global Change Biology*, **22**, 4048-4066.

- Herrero J., Polo M.J., Eugster W., (2016), Evaporesublimation from the snow in the Mediterranean mountains of Sierra Nevada (Spain), *Cryosphere*, **10**.
- Hiyama T., Strunin M., Tanaka H., Ohta T., (2007), The development of local circulations around the Lena River and their effect on tower-observed energy imbalance, *Hydrological Processes: An International Journal*, **21**, 2038-2048.
- Horst T., Oncley S., (2006), Corrections to inertial-range power spectra measured by CSAT3 and Solent sonic anemometers, 1. Path-averaging errors, *Boundary-Layer Meteorology*, **119**, 375-395.
- Jackson S.I., Prowse T.D., (2009), Spatial variation of snowmelt and sublimation in a high-elevation semi-desert basin of western Canada, *Hydrological Processes: An International Journal*, **23**, 2611-2627.
- Jennings K.S., Kittel T.G., Molotch N.P., (2018), Observations and simulations of the seasonal evolution of snowpack cold content and its relation to snowmelt and the snowpack energy budget, *The Cryosphere*, **12**.
- Jin H., Yu Q., Lü L., Guo D., He R., Yu S., Sun G., Li Y., (2007), Degradation of permafrost in the Xing'anling Mountains, Northeastern China, *Permafrost and Periglacial Processes*, **18**, 245-258.
- Jones M.F., Castonguay M., Nasr M., Ogilvie J., Arp P.A., Bhatti J., (2014), Modeling hydrothermal regimes and potential impacts of climate change on permafrost within the South Mackenzie Plain, Northwest Territories, Canada, *Écoscience*, **21**, 21-33.
- Kelliher F., Hollinger D., Schulze E.D., Vygodskaya N., Byers J., Hunt J., McSeveny T., Milukova I., Sogatchev A., Varlargin A., (1997), Evaporation from an eastern Siberian larch forest, *Agricultural and Forest Meteorology*, **85**, 135-147.
- Kokelj S., Palmer M., Lantz T., Burn C.R., (2017), Ground temperatures and permafrost warming from forest to tundra, Tuktoyaktuk Coastlands and Anderson Plain, NWT, Canada, *Permafrost Periglac*, **28**, 543-551.
- Lewkowicz A.G., (2008), Evaluation of miniature temperature-loggers to monitor snowpack evolution at mountain permafrost sites, northwestern Canada, *Permafrost and Periglacial Processes*, **19**, 323-331.
- Li F., Zhou G., Cao M., (2006), Responses of Larix gmelinii geographical distribution to future climate change: A simulation study, *Journal of Applied Ecology*, **17**, 2255-2260.
- Li H., Guan D., Wang A., Wu J., Jin C., Shi T., (2013), Characteristics of evaporation over broadleaved Korean pine forest in Changbai Mountains, Northeast China during snow cover period in winter, *Chinese Journal of Applied Ecology*, **24**, 1039-1044
- Li H., Wang A., Guan D., Jin C., Wu J., Yuan F., Shi T., (2016), Empirical model development for ground snow sublimation beneath a temperate mixed forest in Changbai mountain, *Journal of Hydrologic Engineering*, **21**, 04016040, doi:10.1061/(ASCE)HE.1943-5584.0001415.
- Liao J., Shen G., Li Y., (2013), Lake variations in response to climate change in the Tibetan Plateau in the past 40 years, *International Journal of Digital Earth*, **6**, 534-549.
- Lundberg A., Halldin S., (1994), Evaporation of intercepted snow: Analysis of governing factors, *Water Resources Research*, **30**, 2587-2598.
- Lundberg A., Calder I., Harding R., (1998), Evaporation of intercepted snow: measurement and modelling, *Journal of Hydrology*, **206**, 151-163.
- Lundberg A., Koivusalo H., (2003), Estimating winter evaporation in boreal forests with operational snow course data, *Hydrological Processes*, **17**, 1479-1493.
- Male D.H., Granger R.J., (1981), Snow surface energy exchange, *Water Resources Research*, **17**, 609-627.
- MacDonald M.K., Pomeroy J.W., Essery R.L., (2018), Water and energy fluxes over northern prairies as affected by chinook winds and winter precipitation, *Agricultural and Forest Meteorology*, **248**, 372-385.
- McCaughy J., Saxton W., (1988), Energy balance storage terms in a mixed forest, *Agricultural and Forest Meteorology*, **44**, 1-18.
- Minderlein S., Menzel L., (2015), Evapotranspiration and energy balance dynamics of a semi-arid mountainous steppe and shrubland site in Northern Mongolia, *Environmental Earth Sciences*, **73**, 593-609.
- Mölder M., Grelle A., Lindroth A., Halldin S., (1999), Flux-profile relationships over a boreal forest-roughness sublayer corrections, *Agricultural and Forest Meteorology*, **98**, 645-658.
- Molotch N.P., Blanken P.D., Williams M.W., Turnipseed A.A., Monson R.K., Margulis S.A., (2007), Estimating sublimation of intercepted and sub-canopy snow using eddy covariance systems, *Hydrological Processes: An International Journal*, **21**, 1567-1575.
- Nakai T., Van der Molen M., Gash J., Kodama Y., (2006), Correction of sonic anemometer angle of attack errors, *Agricultural and Forest Meteorology*, **136**, 19-30.
- Nakai Y., Sakamoto T., Terajima T., Kitamura K., Shirai T., (1999), The effect of canopy-snow on the energy balance above a coniferous forest, *Hydrological Processes*, **13**, 2371-2382.
- Nelson K., Kurc S.A., John G., Minor R., Barron-Gafford G. A., (2014), Influence of snow cover duration on soil evaporation and respiration efflux in mixed-conifer ecosystems, *Ecohydrology*, **7**, 869-880.
- Ohta T., Hiyama T., Tanaka H., Kuwada T., Maximov T.C., Ohata T., Fukushima Y., (2001), Seasonal variation in the energy and water exchanges above and below a larch forest in eastern Siberia, *Hydrological Processes*, **15**, 1459-1476.
- Oliphant A., Grimmond C., Zutter H., Schmid H., Su H.B., Scott S., Offerle B., Randolph J., Ehman J., (2004), Heat storage and energy balance fluxes for a temperate deciduous forest, *Agricultural and Forest Meteorology*, **126**, 185-201.
- Pal S.K., Wallis S.G., Arthur S., (2018), An assessment of heavy metals pollution potential of road sediment derived from a suburban road network under different weather conditions, *Environmental Engineering and Management Journal*, **17**, 1955-1966.
- Perez P.J., Castellvi, F., Martínez-Cob A., (2008), A simple model for estimating the Bowen ratio from climatic factors for determining latent and sensible heat flux, *Agricultural and Forest Meteorology*, **148**, 25-37.
- Pérez-Palazón M., Pimentel R., Herrero J., Aguilar C., Perales J., Polo M., (2015), Extreme values of snow-related variables in Mediterranean regions: trends and long-term forecasting in Sierra Nevada (Spain), *Proceedings of the International Association of Hydrological Sciences*, **369**, 157-162.
- Phillips M., Schweizer J., (2007), Effect of mountain permafrost on snowpack stability, *Cold Regions Science and Technology*, **47**, 43-49.
- Pomeroy J.W., Dion K., (1996), Winter radiation extinction and reflection in a boreal pine canopy: measurements and modelling, *Hydrological Processes*, **10**, 1591-1608.

- Pomeroy J., Parviainen J., Hedstrom N., Gray D., (1998), Coupled modelling of forest snow interception and sublimation, *Hydrological processes*, **12**, 2317-2337.
- Roth T.R., Nolin A.W., (2017), Forest impacts on snow accumulation and ablation across an elevation gradient in a temperate montane environment, *Hydrology and Earth System Sciences*, **21**, 5427-5442.
- Saitoh T.M., Tamagawa I., Muraoka H., Koizumi H. (2011), Energy balance closure over a cool temperate forest in steeply sloping topography during snowfall and snow-free periods. *Journal of Agricultural Meteorology*, 1103090078-1103090078.
- Schmid H.P., Grimonid C.S.B., Cropley F., Offerle B., Su H.B., (2000), Measurements of CO₂ and energy fluxes over a mixed hardwood forest in the mid-western United States, *Agricultural and Forest Meteorology*, **103**, 357-374.
- Sexstone G.A., (2016), Snow sublimation and seasonal snowpack variability, *Colorado State University*.
- Smith S.L., Riseborough D.W., Bonnaventure P.P., (2015), Eighteen year record of forest fire effects on ground thermal regimes and permafrost in the Central Mackenzie Valley, NWT, Canada, *Permafrost and Periglacial Processes*, **26**, 289-303.
- Storck P., Lettenmaier D.P., Bolton S.M., (2002), Measurement of snow interception and canopy effects on snow accumulation and melt in a mountainous maritime climate, Oregon, United States, *Water Resources Research*, **38**, 5-1-5-16.
- Talbot C.A., Ogden F.L., Or D., (2004), Comment on "Layer averaged Richards' equation with lateral flow" by Praveen Kumar, *Advances in Water Resources*, **10**, 1041-1042.
- Tanaka H., Hiyama T., Kobayashi N., Yabuki H., Ishii Y., Desyatkin R. V., Maximov T.C., Ohta T., (2008), Energy balance and its closure over a young larch forest in eastern Siberia, *Agricultural and Forest Meteorology*, **148**, 1954-1967.
- Tetzlaff D., Buttle J., Carey S.K., Van Huijgevoort M.H., Laudon H., McNamara J.P., Mitchell C.P., Spence C., Gabor R.S., Soulsby C., (2015), A preliminary assessment of water partitioning and ecohydrological coupling in northern headwaters using stable isotopes and conceptual runoff models, *Hydrological Processes*, **29**, 5153-5173.
- Tor-ngern P., Oren R., Palmroth S., Novick K., Oishi A., Linder S., Ottosson-Löfvenius M., Näsholm T., (2018), Water balance of pine forests: Synthesis of new and published results, *Agricultural and Forest Meteorology*, **259**, 107-117.
- Turnipseed A., Blanken P., Anderson D., Monson R.K., (2002), Energy budget above a high-elevation subalpine forest in complex topography, *Agricultural and Forest Meteorology*, **110**, 177-201.
- Varhola A., Coops N.C., Weiler M., Moore R.D., (2010), Forest canopy effects on snow accumulation and ablation: An integrative review of empirical results, *Journal of Hydrology*, **392**, 219-233.
- Wang R., Kumar M., Marks D., (2013), Anomalous trend in soil evaporation in a semi-arid, snow-dominated watershed, *Advances in Water Resources*, **57**, 32-40.
- Wilson K., Goldstein A., Falge E., Aubinet M., Baldocchi D., Berbigier P., Bernhofer C., Ceulemans R., Dolman H., Field C., (2002), Energy balance closure at FLUXNET sites, *Agricultural and Forest Meteorology*, **113**, 223-243.
- Winkler R., Spittlehouse D., Golding D., (2005), Measured differences in snow accumulation and melt among clearcut, juvenile, and mature forests in southern British Columbia, *Hydrological Processes: An International Journal*, **19**, 51-62.
- Xu W., Ma L., Ma M., Zhang H., Yuan W., (2017), Spatial-temporal variability of snow cover and depth in the Qinghai-Tibetan Plateau, *Journal of Climate*, **30**, 1521-1533.
- Xu Z., Liu S., Gong L., Wang J., Li X., (2008), A study on the data processing and quality assessment of the eddy covariance system, *Advances in Earth Science*, **4**.
- Yi L., Ti-jiu C., Hou-cai S., Zheng Y., (2014), Characteristics of the Snow Interception and the Snowpack in Scotch Pine Forest in Great Xing'an Mountains, *Journal of Soil and Water Conservation*, **22**.
- Zhang Y., Ohata T., Ersi K., Tandong Y., (2003), Observation and estimation of evaporation from the ground surface of the cryosphere in eastern Asia, *Hydrological Processes*, **17**, 1135-1147.